Electronic Supplementary Material (ESI) for ChemComm.

One-step side-by-side 3D printing constructing linear full batteries

Junwei Ding[1, 2, *], Huaiyang Zheng[2], and Xiaoyan Ji[1, *]

Energy Engineering, Division of Energy Science, Lulea University of Technology, 97187 Lulea, Sweden. Email: xiaoyan.ji@ltu.se
College of Materials and Chemical Engineering, Zhengzhou University of Light Industry, Zhengzhou 450002, China. Email: dingjunwei@zzuli.edu.cn

Experimental section

Preparation of cathode and anode electrode inks

For LIBs, the mesocarbon microbeads (MCMB)/lithium titanium oxide ($Li_4Ti_5O_{12}$) and lithium iron phosphate ($LiFePO_4$) were used as the anode and cathode, respectively. The MCMB/$Li_4Ti_5O_{12}$ and $LiFePO_4$ inks were prepared by blending the MCMB/$Li_4Ti_5O_{12}$/$LiFePO_4$, Super P (conductive agent), and poly (vinyl difluoride) (PVDF, binding agent) with 80:10:10 (weight percentage, wt.%). For example, to synthesize the $Li_4Ti_5O_{12}$ ink, 1600 mg $Li_4Ti_5O_{12}$, 200 mg Super P, and 200 mg PVDF were ground in an agate mortar for 15~20 min. Then, N-methyl-pyrrolidone (NMP, 5.2 mL) was added. Finally, the above mixture was ground for 30 min to obtain the $Li_4Ti_5O_{12}$ ink. For the fabrication of $LiFePO_4$ ink, 1600 mg $LiFePO_4$, 200 mg Super P, and 200 mg PVDF were ground for 15~20 min. Then, 3 mL NMP was added. The above mixture was ground for 30 min to obtain the $LiFePO_4$ ink.

For SIBs, similar to the preparation of $Li_4Ti_5O_{12}$ and $LiFePO_4$ inks, the $Na_3V_2(PO_4)_3$ ink was also fabricated via blending $Na_3V_2(PO_4)_3$, Super P, and PVDF with 80:10:10 (wt.%).

For AZIBs, similar to the preparation of $Li_4Ti_5O_{12}$ and $LiFePO_4$ inks, the zinc anode and VO_2(B) cathode inks were also prepared via blending the commercial zinc powders/ VO_2(B), Super P, and PVDF with 80:10:10 (wt.%).

Preparation of the electrolyte (separator) ink

The electrolyte(separator) ink was fabricated by blending the poly (methyl methacrylate) (molecular weight is about 350,000), silicon dioxide (the size is about 15 nm), and N, N-dimethylformamide. Typically, 2000 mg poly (methyl methacrylate) and 900 mg silicon dioxide were added into 10 mL N, N-dimethylformamide. Then, the above mixture was stirred for 1440 min at 25 ℃.

One-step side-by-side 3D-printing constructing batteries

The one-step side-by-side 3D printing was conducted on a benchtop robot (F4200N/FISNAR) with three independent air-powered fluid dispensers. The 3D printed linear filaments were dried (80 ℃, 12h) to remove N-methyl-pyrrolidone and N, N-dimethylformamide. The thickness of the prepared linear full cells is about 3.5 millimeters, which is thicker than conventional batteries. The applied current collector was polyethylene terephthalate (PET). Then, the liquid electrolytes were injected to obtain LIBs, SIBs and AZIBs. The encapsulation of LIBs and SIBs was conducted in an argon-filled glove box, while that of AZIBs was conducted in the ambient environment. The adhesion of the pastes onto different substrates is various. The adhesion between pastes and PET is stronger than that of the gilded quartz glass due to the interaction between PET and the ink solvent. The conductive silver paste can be used to increase the adhesion between pastes and substrates.

Characterization

The rheological curves of inks were performed on the AR 2000 rheometer (TA Instruments) with the flat steel plate (2 cm) at 25 °C. The structural and morphological information of samples was obtained via X-ray diffraction (XRD, Bruker D8 Advance) and scanning electron microscopy (SEM, JEOL 7500), respectively.

Electrochemical Measurements

For LIBs, the $Li_4Ti_5O_{12}$ and $LiFePO_4$ half-batteries were tested with the voltage ranges of 1.0-2.5 V and 2.0-4.0 V, respectively. The full-batteries of $Li_4Ti_5O_{12}$ and $LiFePO_4$ were tested at 1.0-3.0 V. Meanwhile, the MCMB half-batteries were tested with the voltage range of 0.01-2.5 V. The corresponding full-batteries matched with $LiFePO_4$ were tested at 2.0-4.0 V. 1 M lithium hexafluorophosphate in ethylene carbonate/ethyl methyl carbonate/dimethyl carbonate (the volume ratio is 1:1:1) was used as the liquid

electrolyte.

For SIBs, the test ranges were 2.3-3.9 V, 1.3-2.0 V, and 1.0-3.0 V for the cathode-based half-batteries, the anode-based half-batteries, and full-batteries, respectively. 1 M sodium perchlorate in ethylene carbonate/propylene carbonate (the mass ratio is 1:1) with 5 wt. % fluoroethylene carbonate additive was used as the liquid electrolyte.

For AZIBs, the test range was 0.3-1.5 V. The liquid electrolyte was 3 mol L^{-1} zinc trifluoromethanesulfonate ($Zn(CF_3SO_3)_2$) aqueous solution.

Battery cyclic voltammetry (CV) and charge/discharge tests were tested on the CHI 660D workstation and Land CT2001A system, respectively. The full-battery capacities of LIBs, SIBs, and AZIBs were based on the total mass of the anode, cathode, and electrolyte (liquid electrolytes were excluded).

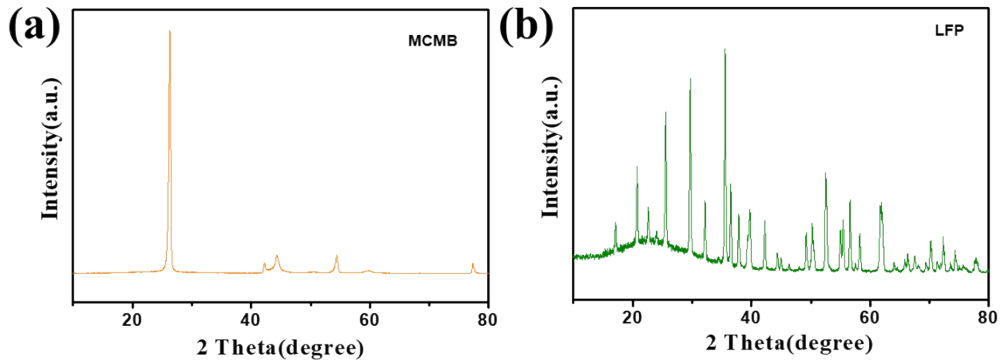

Figure S1. XRD patterns of (a) MCMB and (b) LFP. The used LFP is same as that we previously reported coaxial 3D printing [1].

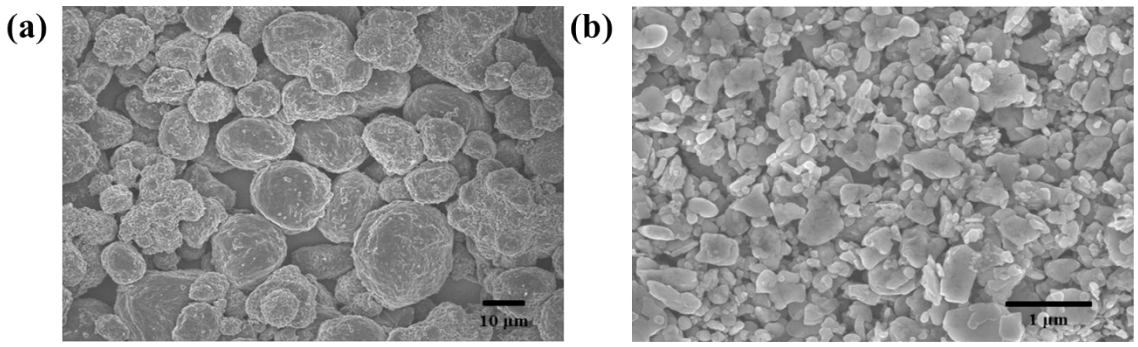

Figure S2. SEM images of (a) MCMB and (b) LFP, showing that MCMB and LFP have different particle sizes.

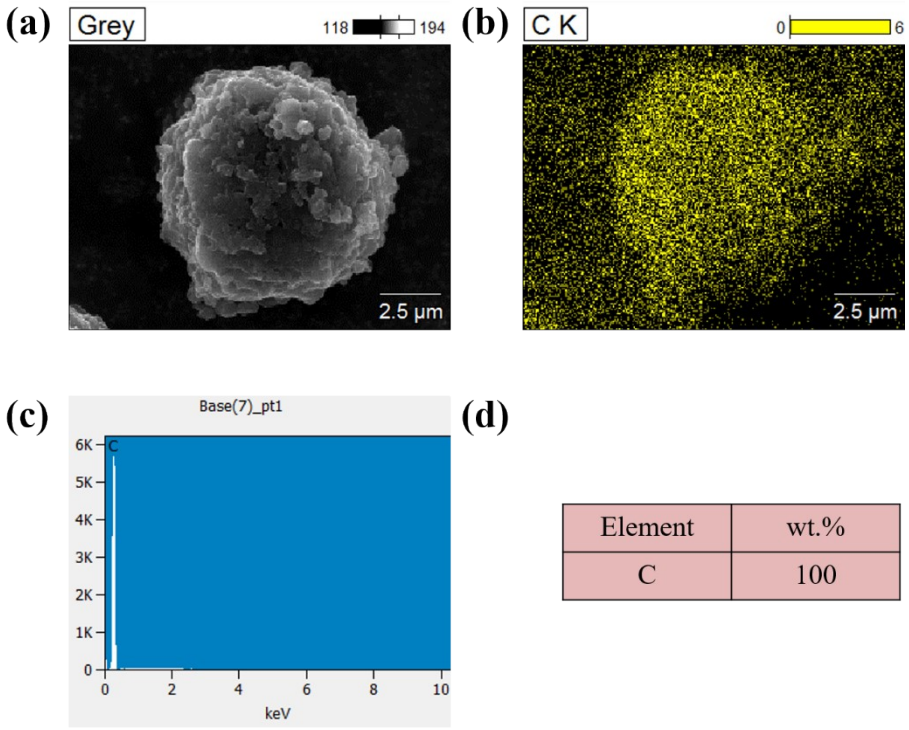

Element	wt.%
C	100

Figure S3. (a) SEM image, (b) mapping energy dispersive spectroscopy (EDS), (c) line EDS, and (d) element percentage of MCMB. It can be seen that MCMB is spherical in morphology with a particle size of several micrometers. The corresponding energy spectra and element distribution indicate that MCMB is composed of the carbon element.

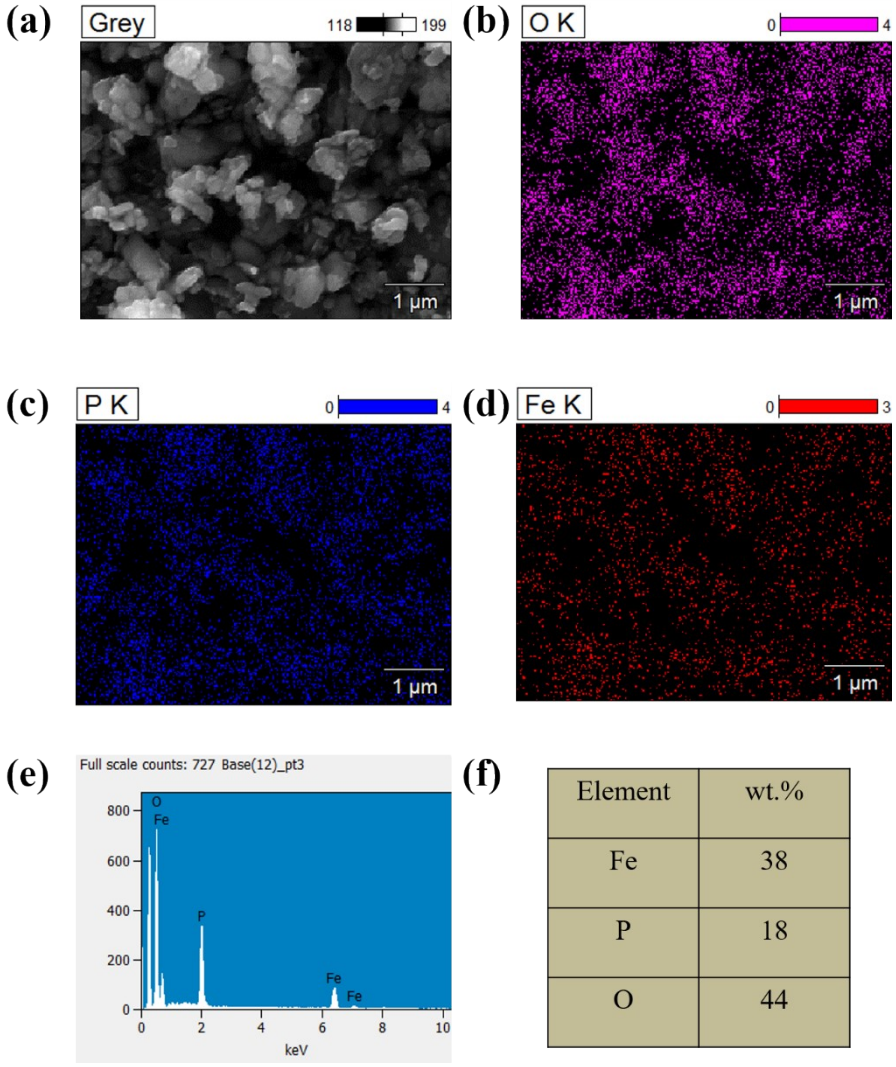

Element	wt.%
Fe	38
P	18
O	44

Figure S4. (a) SEM image, (b-d) O, P, and Fe mapping EDS, (e) line EDS, and (f) O, P, and Fe element percentage of LFP. LFP has an irregular morphology. It can be seen from the element distribution spectra that LFP is mainly composed of iron, phosphorus, and oxygen elements. It should be noted that the lithium element cannot be identified in the EDS test.

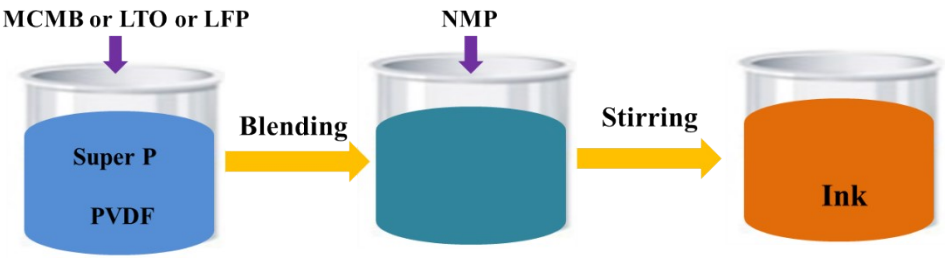

Figure S5. Inks are produced via simple blending of active material, Super P, and PVDF followed by stirring in suitable volume NMP.

Figure S6. Optical image of the side-by-side multi-nozzle.

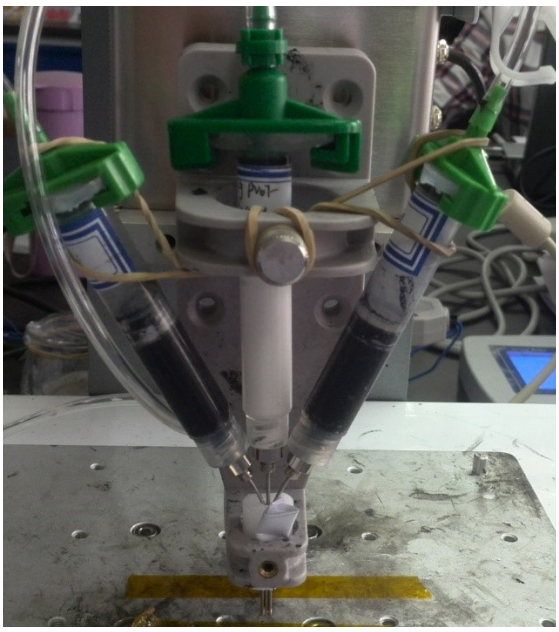

Figure S7. Optical picture of the 3D printer with the side-by-side multi-nozzle.

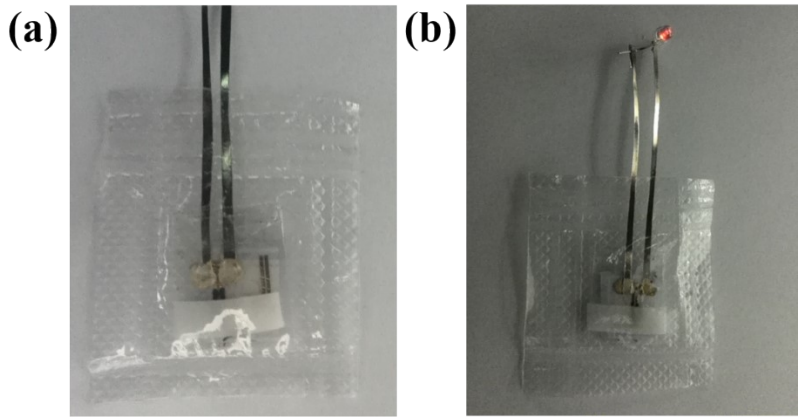

Figure S8. Optical pictures of the 3D printed linear cell (a) with the encapsulation and (b) with one lit light emitting diode (LED).

Figure S9. Optical image of the obtained LTO anode, electrolyte(separator), and LFP cathode filaments on the polyethylene terephthalate (PET) substrate wrapping on people's wrist.

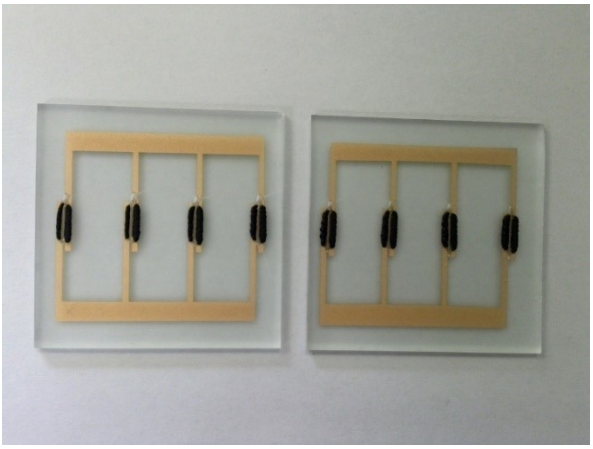

Figure S10. Optical images of the obtained LTO anode, electrolyte(separator), and LFP cathode filaments on the gilded quartz glass substrate with the parallel circuit structure.

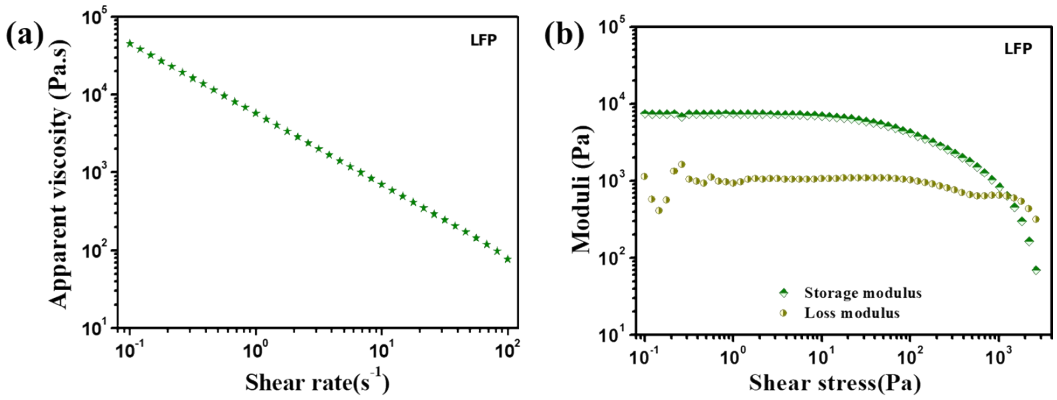

Figure S11. (a) Viscosity versus shear rate and (b) storage/loss moduli versus shear stress of the LFP ink. The applied LFP ink is same as that we previously reported coaxial 3D printing [1].

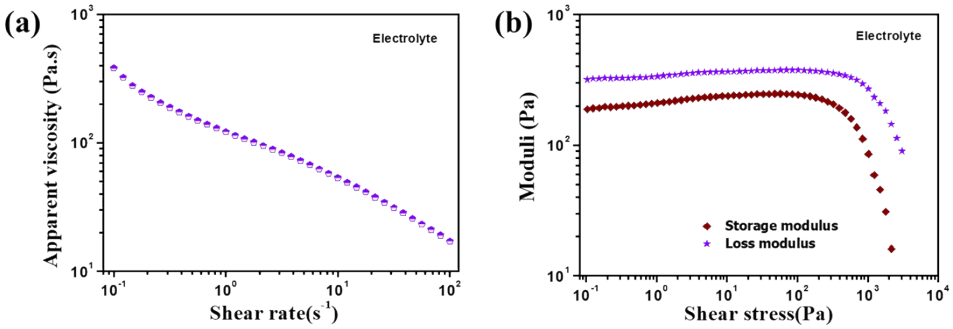

Figure S12. (a) Viscosity versus shear rate and (b) storage/loss moduli versus shear stress of the polymer-based electrolyte ink. The applied electrolyte (separator) ink is same as that we previously reported coaxial 3D printing [1].

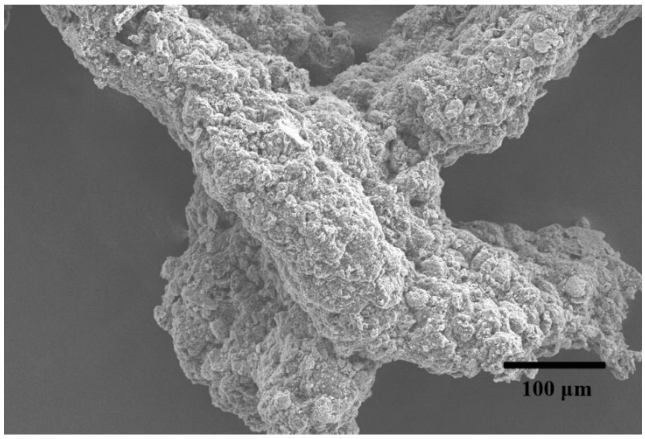

Figure S13. SEM of two NVP electrode layers via the side-by-side 3D printing. The layer-by-layer printing via the side-by-side nozzles can be achieved. At present, one-step side-by-side 3D printing with multi-layer structures cannot solve the problems of gravity-induced adhesion and structural collapse between different layers. Achieving side-by-side printing of battery components and coaxial printing of encapsulation materials at the same time is a promising approach to solve the current problems.

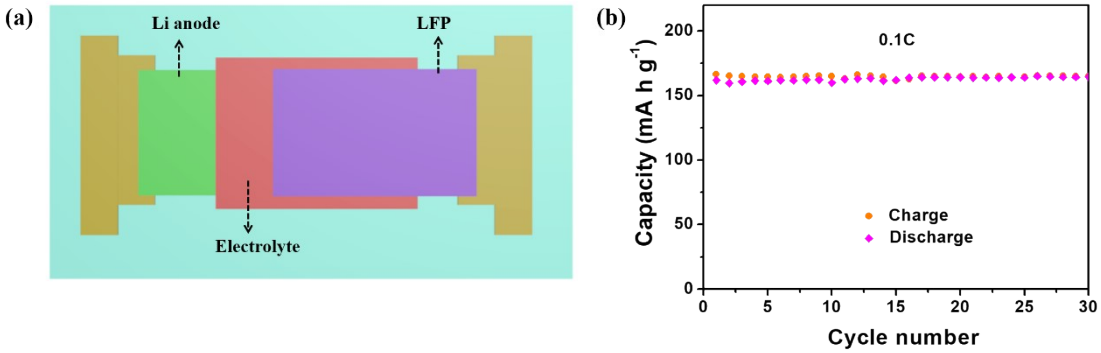

Figure S14. (a, b) Structural diagram and the cycle performance of the LFP half batteries at 0.1 C (1C is equal to 170 mA h g^{-1}).

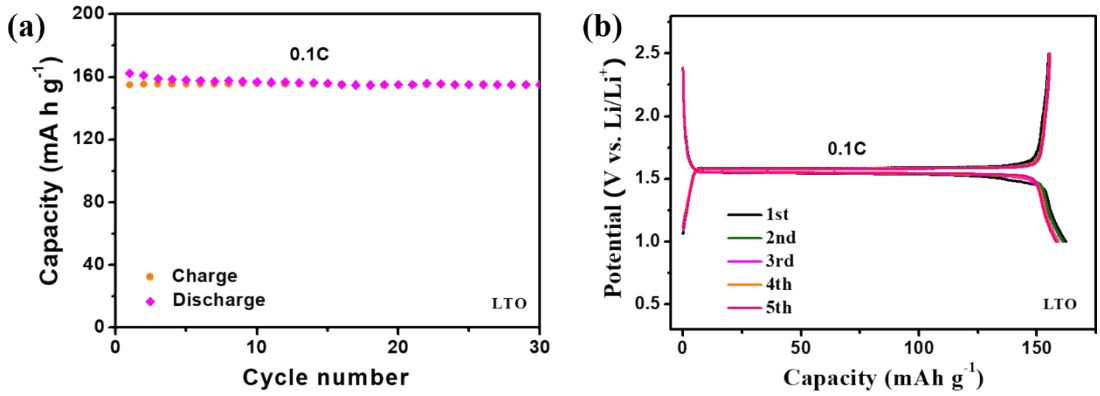

Figure S15. (a, b) Cycle performance and the corresponding voltage-capacity curves of the LTO half batteries at 0.1 C (1C is equal to 170 mA h g^{-1}).

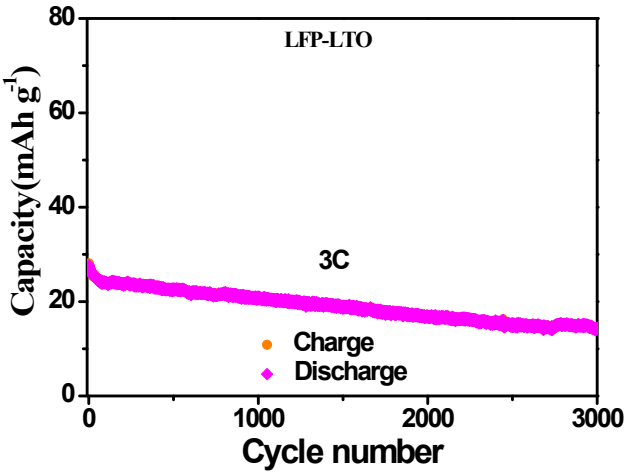

Figure S16. The long cycle performance of the LFP-LTO full batteries at 3 C (1C is equal to 170 mA h g^{-1}).

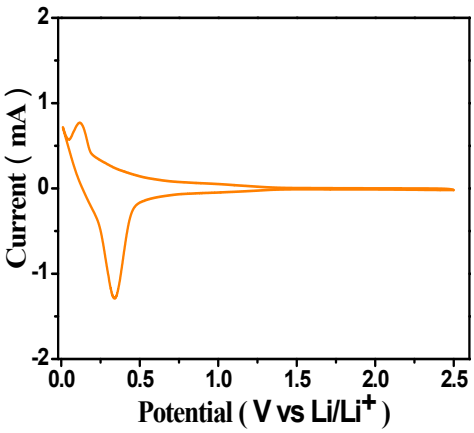

Figure S17. CV curve of the MCMB-based half batteries.

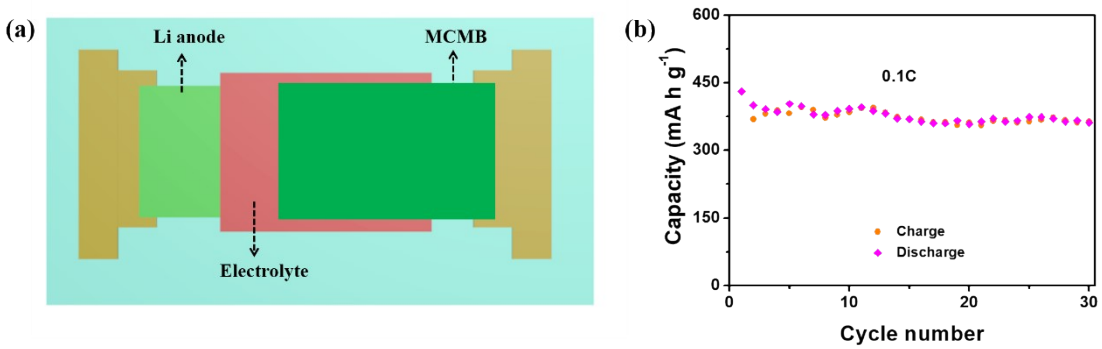

Figure S18. (a, b) Structural diagram and the cycle performance of the MCMB half batteries at 0.1 C (1C is equal to 170 mA h g^{-1}).

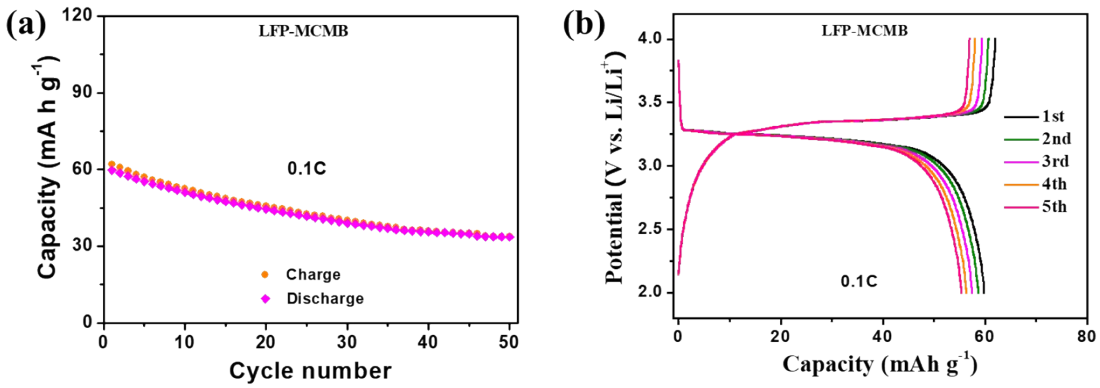

Figure S19. (a, b) Cycle performance and the corresponding voltage-capacity curves of the LFP-MCMB full batteries at 0.1 C (1C is equal to 170 mA h g^{-1}).

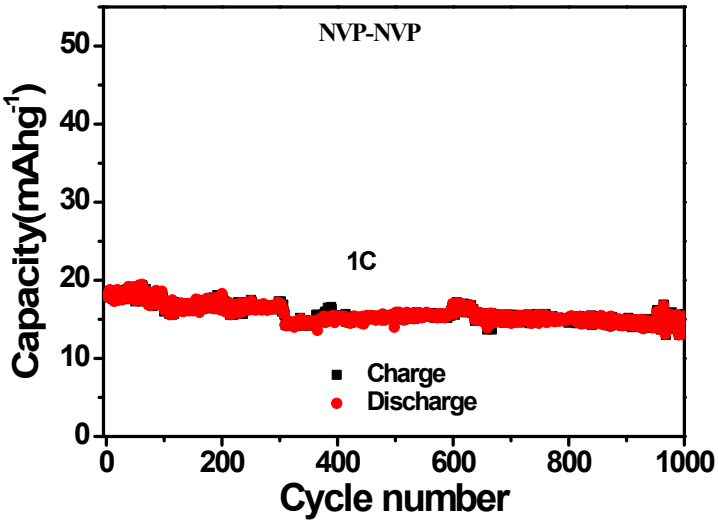

Figure S20. The long cycle performance of the NVP-NVP full batteries at 1C (1C is equal to 117.6 mA h g^{-1}).

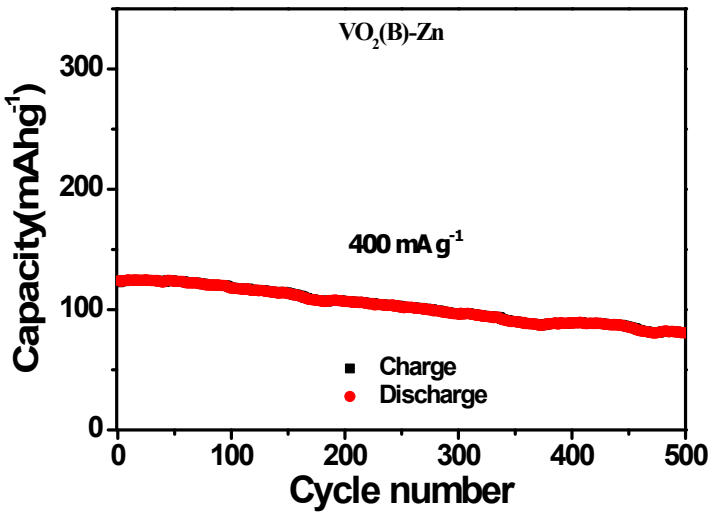

Figure S21. The long cycle performance of the VO_2(B)-Zn powders full batteries at 400 mA g^{-1}.

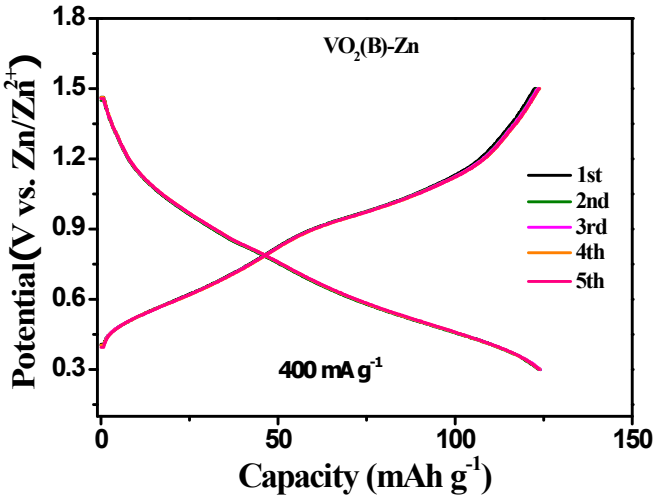

Figure S22. The corresponding voltage-capacity curves of the VO_2(B)-Zn powders full batteries at 400 mA g^{-1}.

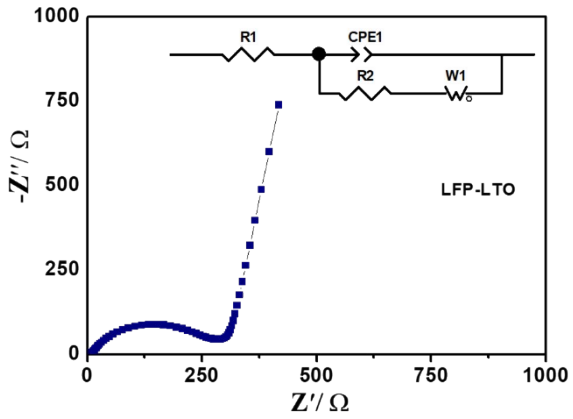

Figure S23. The impedance spectrum for LFP and LTO based lithium-ion full battery. Inset: the equivalent circuit *(R1*: solution resistance; *R2*: charge-transfer resistance; *CPE1*: constant-phase element; *W1*: Warburg diffusion process). The charge-transfer resistance is 255 Ω, which indicates that the ion diffusion at cathode-electrolyte-anode interfaces is comparable with regular coin cells.

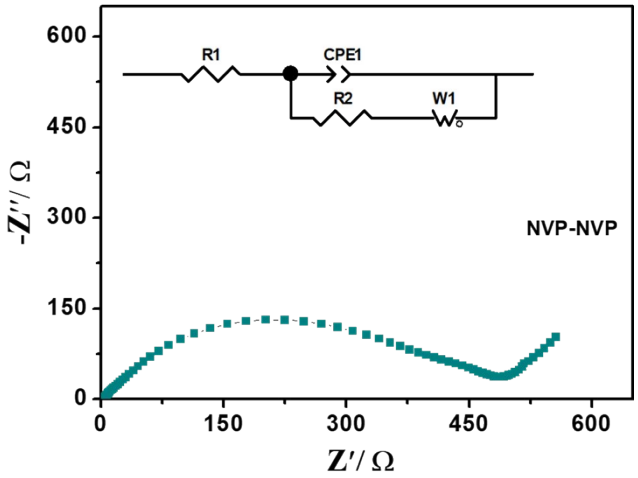

Figure S24. The impedance spectrum for NVP based sodium-ion full battery. Inset: the equivalent circuit. The charge-transfer resistance is 435 Ω, which indicates that the ion diffusion at cathode-electrolyte-anode interfaces is comparable with regular coin cells.

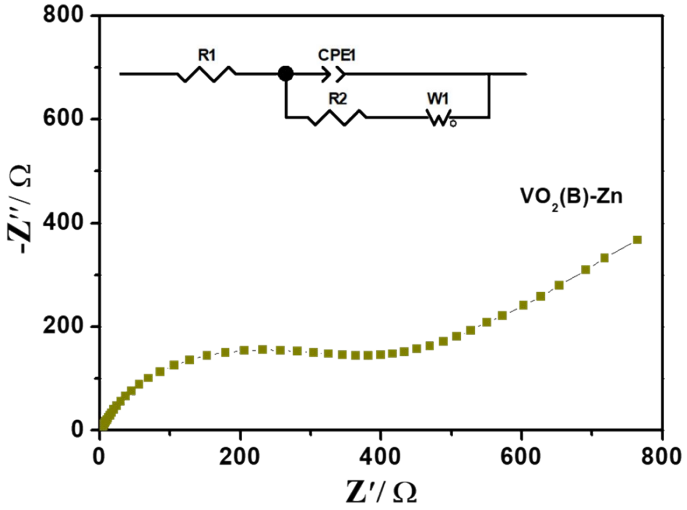

Figure S25. The impedance spectrum for VO_2(B) and zinc based zinc-ion full battery. Inset: the equivalent circuit. The charge-transfer resistance is 289 Ω, which indicates that the ion diffusion at cathode-electrolyte-anode interfaces is comparable with regular coin cells.

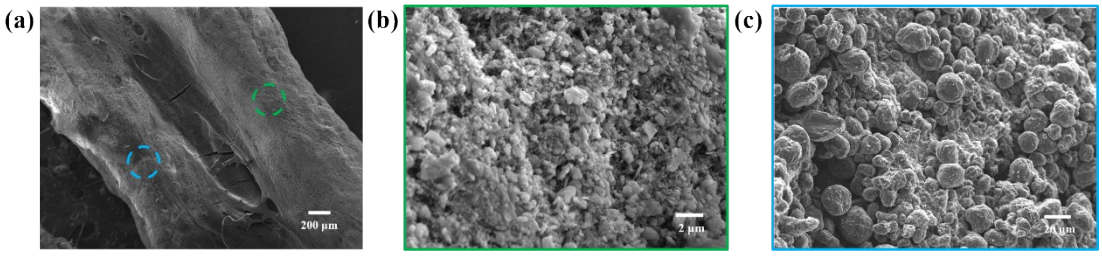

Figure S26. (a-c) SEM images with different resolutions for LFP and MCMB based lithium-ion full battery after 50 cycles. It can be seen that the linear lithium-ion full battery can maintain the initial structure. The corresponding enlarged SEM images show that the electrode components are in close contact.

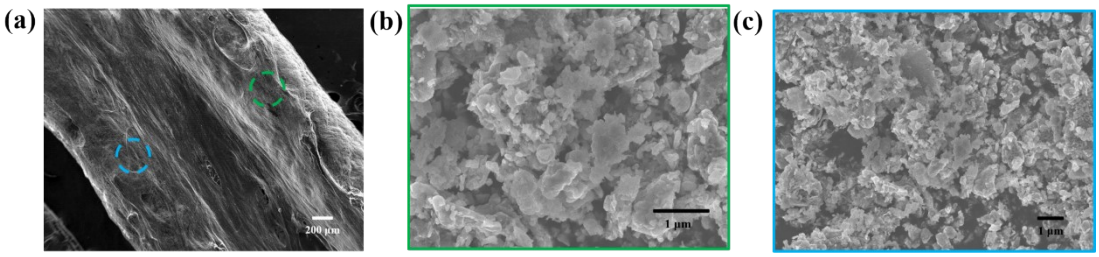

Figure S27. (a-c) SEM images with different resolutions for NVP based sodium-ion full battery after 50 cycles. The linear sodium-ion full battery can maintain the pristine structure. The corresponding enlarged SEM images show that the electrode components are in close contact.

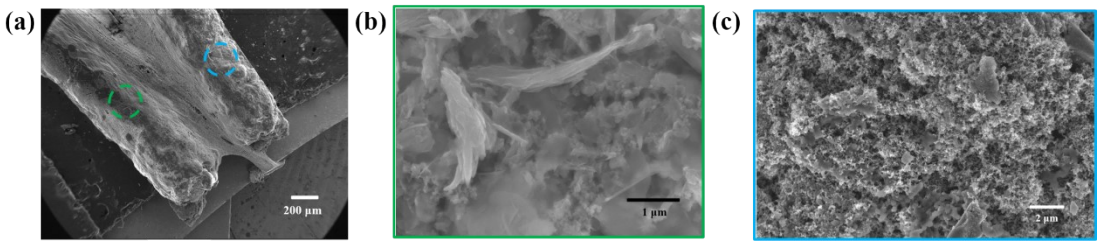

Figure S28. (a-c) SEM images with different resolutions for zinc-ion full battery after 50 cycles. The linear zinc-ion full battery can maintain the original structure. The corresponding enlarged SEM images show that the electrode components are in close contact. It should be noted that the formation of sheet-like basic zinc trifluoromethanesulfonate is inevitable in the aqueous zinc-ion battery using zinc trifluoromethanesulfonate electrolyte, which corresponds to the sheet-like material in the enlarged SEM images.

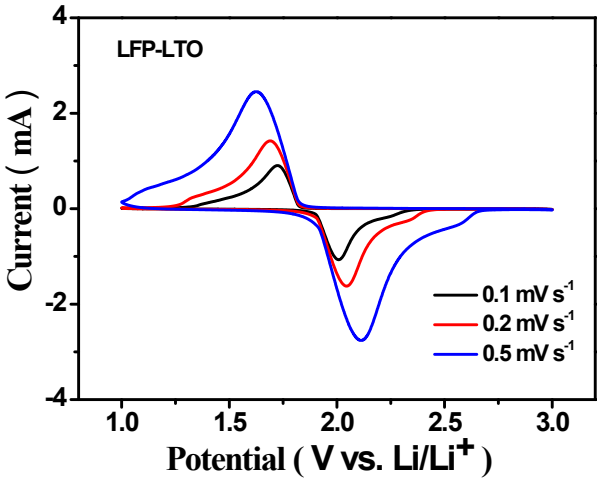

Figure S29. CV curves with different scan rates for LFP and LTO based lithium-ion full battery. The redox peaks in CV curves are consistent with the battery charge/discharge platforms in the constant current charge/discharge test.

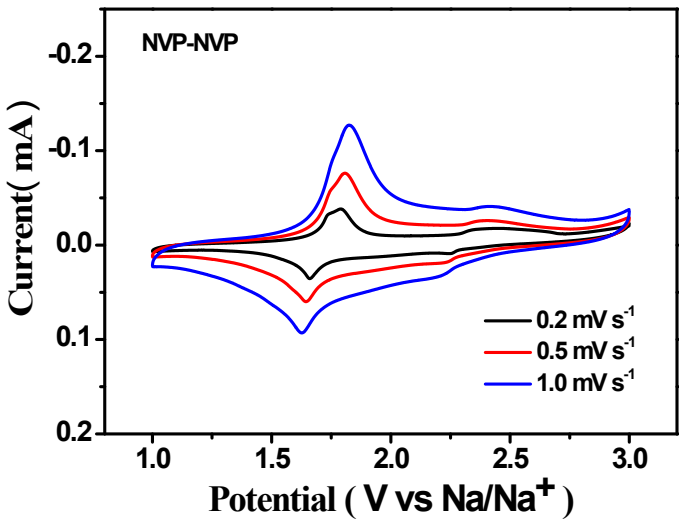

Figure S30. CV curves with different scan rates for NVP based sodium-ion full battery.

The CV redox peaks are consistent with the full battery charge/discharge platforms.

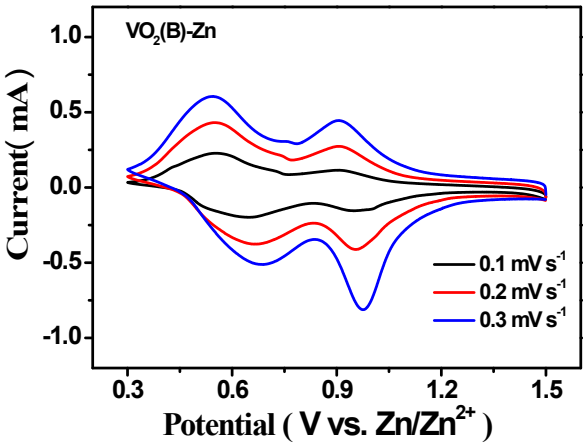

Figure S31. CV curves with different scan rates for VO_2(B) and zinc based zinc-ion full battery.

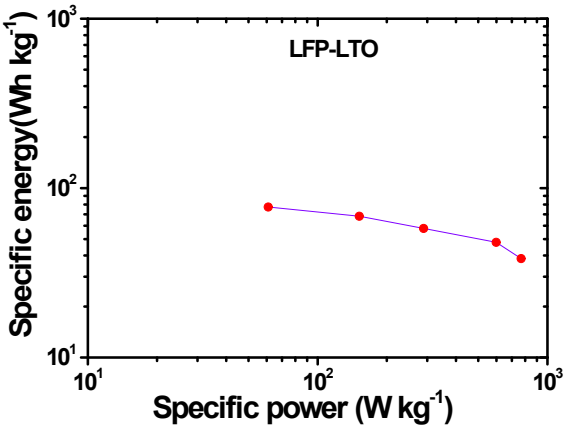

Figure S32. Ragone plot of the LFP and LTO based lithium-ion full battery. The energy and power densities were based on the total mass of the LTO anode, LFP cathode, and electrolyte (liquid electrolytes were excluded).

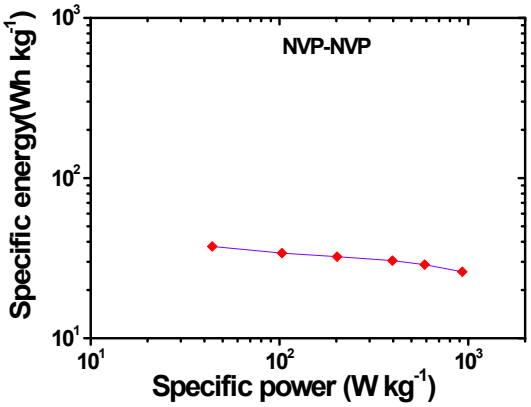

Figure S33. Ragone plot of the NVP based sodium-ion full battery. The energy and power densities were based on the total mass of the NVP anode, NVP cathode, and electrolyte (liquid electrolytes were excluded).

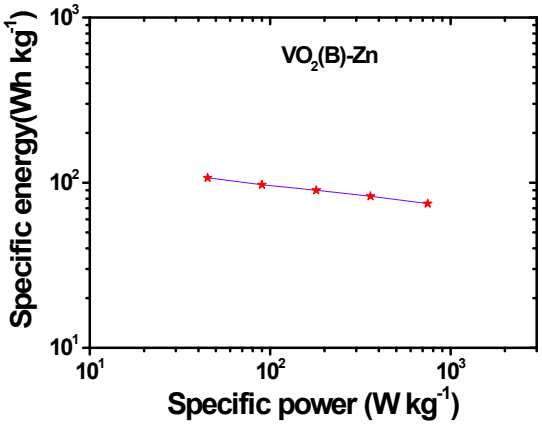

Figure 34. Ragone plot of VO_2(B) and zinc based zinc-ion full battery. The energy and power densities were based on the total mass of the zinc anode, VO_2(B) cathode, and electrolyte (liquid electrolytes were excluded).

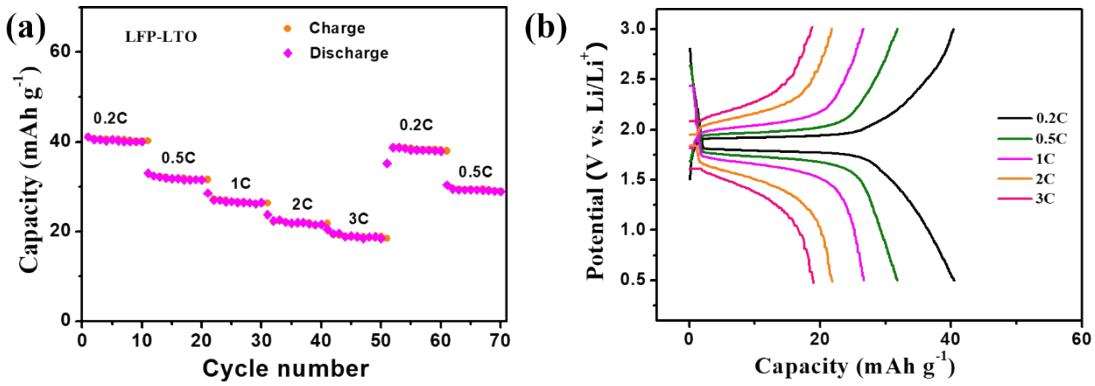

Figure S35. (a, b) Rate performance and the corresponding voltage-capacity curves of the linear LFP-LTO full battery with the 15 degree bending angle (the length is about 1 cm).

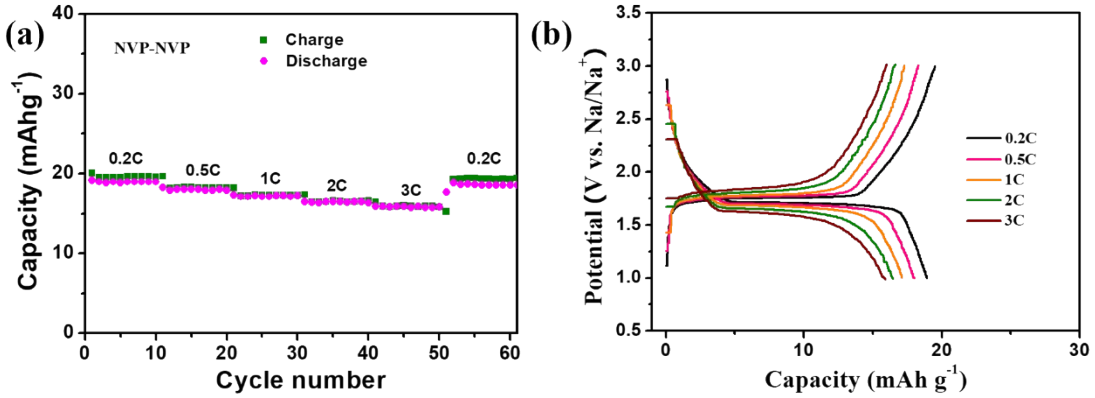

Figure S36. (a, b) Rate performance and the corresponding voltage-capacity curves of the linear NVP-NVP full battery with the 15 degree bending angle (the length is about 1 cm).

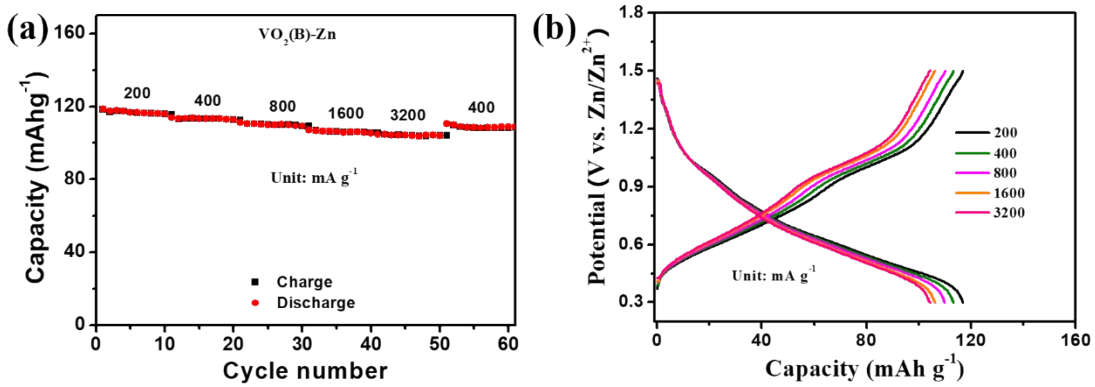

Figure S37. (a, b) Rate performance and the corresponding voltage-capacity curves of the linear VO_2(B)-zinc full battery with the 15 degree bending angle (the length is about 1 cm).

Table S1 The comparison of battery performance via different types of 3D printing.

Battery type	Cathode material	Anode material	Max. current ($A\ g^{-1}$)	Max. capacity ($mA\ h\ g^{-1}$)	Max. cycling-life (cycles)	Ref.
LIBs (full-cell)	LFP	LTO	0.05	100	10	[2]
LIBs (full-cell)	LFP	LTO	N/A	1.5 $mAh\ cm^{-2}$	30	[3]
LIBs (full-cell)	LFP	LTO	0.016	95	2	[4]
LIBs (half-cell)	LFP	Lithium foil	0.85	160_{LFP}	100	[5]
LIBs (half-cell)	$LiMn_{0.21}Fe_{0.79}PO_4$ (LMFP)	Lithium foil	17	161_{LMFP}	1000	[6]
LIBs (half-cell)	LTO	Lithium foil	0.875	150_{LTO}	100	[7]
LIBs (half-cell)	Graphene-polylactic acid	Lithium foil	0.2	20	120	[8]
LIBs (full-cell)	LFP	LTO	0.05	110	30	[9]
SIBs (half-cell)	MoS_2-graphene	Sodium foil	1	300	100	[10]
SIBs (full-cell)	$NaMnO_2$	TiO_2	0.168	84	1000	[11]
AZIBs (half-cell)	$Fe_5V_{15}O_{39}(OH)_9 \cdot 9H_2O$ (FeVO)	Zinc foil	2	350_{FeVO}	675	[12]
LIBs (full-cell)	LFP	LTO	0.51	54.5	3000	**This work**
SIBs (full-cell)	NVP	NVP	0.588	24.2	1000	**This work**
AZIBs (half-cell)	VO_2(B)	Zinc powders	3.2	154.2	500	**This work**

References

[1] D. Ji, H. Zheng, H. Zhang, W. Liu, J. Ding, Coaxial 3D-printing constructing all-in-one fibrous lithium-, sodium-, and zinc-ion batteries, Chem. Eng. J. (2021) 133815. https://doi.org/10.1016/j.cej.2021.133815.

[2] K. Fu, Y. Wang, C. Yan, Y. Yao, Y. Chen, J. Dai, S. Lacey, Y. Wang, J. Wan, T. Li, Z. Wang, Y. Xu, L. Hu, Graphene oxide-based electrode inks for 3D-printed lithium-ion batteries, Adv. Mater. 28(13) (2016) 2587-2594. https://doi.org/10.1002/adma.201505391.

[3] K. Sun, T.-S. Wei, B.Y. Ahn, J.Y. Seo, S.J. Dillon, J.A. Lewis, 3D printing of interdigitated Li-ion microbattery architectures, Adv. Mater. 25(33) (2013) 4539-4543. https://doi.org/10.1002/adma.201301036.

[4] M. Cheng, Y. Jiang, W. Yao, Y. Yuan, R. Deivanayagam, T. Foroozan, Z. Huang, B. Song, R. Rojaee, T. Shokuhfar, Y. Pan, J. Lu, R. Shahbazian-Yassar, Elevated-temperature 3D printing of hybrid solid-state electrolyte for Li-ion batteries, Adv. Mater. 30(39) (2018) 1800615. https://doi.org/10.1002/adma.201800615.

[5] A.J. Blake, R.R. Kohlmeyer, J.O. Hardin, E.A. Carmona, B. Maruyama, J.D. Berrigan, H. Huang, M.F. Durstock, 3D printable ceramic-polymer electrolytes for flexible high-performance Li-ion batteries with enhanced thermal stability, Adv. Energy Mater. 7(14) (2017) 1602920. https://doi.org/10.1002/aenm.201602920.

[6] J. Hu, Y. Jiang, S. Cui, Y. Duan, T. Liu, H. Guo, L. Lin, Y. Lin, J. Zheng, K. Amine, F. Pan, 3D-printed cathodes of $LiMn_{1-x}Fe_xPO_4$ nanocrystals achieve both ultrahigh rate and high capacity for advanced lithium-ion battery, Adv. Energy Mater. 6(18) (2016) 1600856. https://doi.org/10.1002/aenm.201600856.

[7] R.R. Kohlmeyer, A.J. Blake, J.O. Hardin, E.A. Carmona, J. Carpena-Núñez, B. Maruyama, J. Daniel Berrigan, H. Huang, M.F. Durstock, Composite batteries: a simple yet universal approach to 3D printable lithium-ion battery electrodes, J. Mater. Chem. A 4(43) (2016) 16856-16864. https://doi.org/10.1039/C6TA07610F.

[8] C.W. Foster, M.P. Down, Y. Zhang, X. Ji, S.J. Rowley-Neale, G.C. Smith, P.J. Kelly, C.E. Banks, 3D printed graphene based energy storage devices, Sci. Rep. 7(1) (2017) 42233. https://doi.org/10.1038/srep42233.

[9] Y. Wang, C. Chen, H. Xie, T. Gao, Y. Yao, G. Pastel, X. Han, Y. Li, J. Zhao, K. Fu, L. Hu, 3D-printed all-fiber Li-ion battery toward wearable energy storage, Adv. Funct. Mater. 27(43) (2017) 1703140. https://doi.org/10.1002/adfm.201703140.

[10] E. Brown, P. Yan, H. Tekik, A. Elangovan, J. Wang, D. Lin, J. Li, 3D printing of hybrid MoS_2-graphene aerogels as highly porous electrode materials for sodium ion battery anodes, Mater. Des. 170 (2019) 107689. https://doi.org/10.1016/j.matdes.2019.107689.

[11] M.P. Down, E. Martínez-Periñán, C.W. Foster, E. Lorenzo, G.C. Smith, C.E. Banks, Next-generation additive manufacturing of complete standalone sodium-ion energy storage architectures, Adv. Energy Mater. 9(11) (2019) 1803019. https://doi.org/10.1002/aenm.201803019.

[12] H. Ma, X. Tian, T. Wang, K. Tang, Z. Liu, S. Hou, H. Jin, G. Cao, Tailoring pore structures of 3D printed cellular high-loading cathodes for advanced rechargeable zinc-ion batteries, Small 17(29) (2021) 2100746. https://doi.org/10.1002/smll.202100746.